Structural analysis of the role of TPX2 in branching microtubule nucleation

Raymundo Alfaro-Aco,[1] Akanksha Thawani,[2] and Sabine Petry[1]

[1]Department of Molecular Biology and [2]Department of Chemical and Biological Engineering, Princeton University, Princeton, NJ 08544

The mitotic spindle consists of microtubules (MTs), which are nucleated by the γ-tubulin ring complex (γ-TuRC). How the γ-TuRC gets activated at the right time and location remains elusive. Recently, it was uncovered that MTs nucleate from preexisting MTs within the mitotic spindle, which requires the protein TPX2, but the mechanism basis for TPX2 action is unknown. Here, we investigate the role of TPX2 in branching MT nucleation. We establish the domain organization of *Xenopus laevis* TPX2 and define the minimal TPX2 version that stimulates branching MT nucleation, which we find is unrelated to TPX2's ability to nucleate MTs in vitro. Several domains of TPX2 contribute to its MT-binding and bundling activities. However, the property necessary for TPX2 to induce branching MT nucleation is contained within newly identified γ-TuRC nucleation activator motifs. Separation-of-function mutations leave the binding of TPX2 to γ-TuRC intact, whereas branching MT nucleation is abolished, suggesting that TPX2 may activate γ-TuRC to promote branching MT nucleation.

Introduction

Microtubules (MTs) serve as key structural elements of cells and form the framework of the mitotic spindle, which segregates chromosomes during cell division. Spindle assembly relies on generating MTs at the right location and time. Although pure α/β-tubulin heterodimers and GTP are sufficient to generate MTs spontaneously in vitro, cells generally require the universal nucleating factor γ-tubulin (γ-TB) to initiate MT formation. In yeast, γ-TB associates with γ-TB complex proteins (GCPs) 2 and 3 to form the γ-TB small complex (γ-TuSC), whereas higher eukaryotes additionally require GCPs 3–6 to assemble the larger γ-TB ring complex (γ-TuRC). Both complexes form a ring-like template and can bind the α-tubulin subunit that defines the new MT minus end (Zheng et al., 1995; Moritz et al., 1998; Oegema et al., 1999; Murphy et al., 2001; Kollman et al., 2010). Surprisingly, purified γ-TB complexes have low MT nucleation activity that does not seem to match the nucleation capacity observed in cells (Oegema et al., 1999). Therefore, factors have been sought that can activate γ-TB complexes for MT nucleation. The kinase NME7 and the centrosomal protein CDK5RAP2 are direct binding partners of γ-TuRC and increase its nucleation activity in vitro by 2.5-fold (Liu et al., 2014) and ∼7-fold (Choi et al., 2010), respectively. CDK5RAP2 activates γ-TuRC via the so-called γ-TuRC nucleation activator motif (γTuNA; CM1 in yeast). A second motif, Spc110/Pcp1 motif (SPM), is present in the yeast spindle-pole body protein Spc110 and leads to activation of γ-TuSC (Lin et al., 2014). Both motifs are conserved in several other proteins and organisms, but the mechanisms by which γTuNA/CM1 and SPMs activate γ-TB complexes remain to be defined. At the same time, the activation potential of these motifs in vitro still cannot account for the nucleation capacity of the centrosome in cells. Furthermore, other γ-TuRC activators must exist for the various acentrosomal MT nucleation pathways, whereas their identity, motifs, and mode of action remain to be determined.

Recently, MTs were observed to originate from preexisting MTs in meiotic *Xenopus* egg extract, which is essential to generate dense, parallel MT bundles as required in the spindle (Petry et al., 2013). Most importantly, the protein complex augmin and the protein "targeting factor for Xklp2" (TPX2) were identified as key molecular players of γ-TB–dependent branching MT nucleation. TPX2 is one of several spindle assembly factors, which are sequestered by importins and released via Ran-GTP in the vicinity of chromosomes (Gruss et al., 2001). A wide variety of interaction partners have been described for TPX2. The N-terminal 42 amino acids of TPX2 interact with and activate Aurora A kinase, which phosphorylates TPX2, among other targets, and thereby stimulates MT generation in *Xenopus* egg extract (Tsai et al., 2003; Eyers and Maller, 2004; Scrofani et al., 2015). TPX2 also interacts with the kinesin Xklp2 (Wittmann et al., 2000) and via its C-terminal 35 amino acids with the antiparallel sliding motor Eg5 (Eckerdt et al., 2008). The Ran-regulated binding of importin α takes place in TPX2's middle region (Schatz et al., 2003). TPX2 also

Correspondence to Sabine Petry: spetry@princeton.edu

Abbreviations used: CD, circular dichroism; EB, end-binding protein; GCP, γ-tubulin complex protein; γ-TB, γ-tubulin; γTuNA, γ-tubulin ring complex nucleation activator; γ-TuRC, γ-tubulin ring complex; γ-TuSC, γ-tubulin small complex; MALS, multiple angle light scattering; MT, microtubule; SEC, size exclusion chromatography; SPM, Spc110/Pcp1 motif; TIRF, total internal reflection.

The Rockefeller University Press $30.00
J. Cell Biol. Vol. 216 No. 4 983–997
https://doi.org/10.1083/jcb.201607060

binds to MTs and is important for spindle assembly (Brunet et al., 2004). Recent in vitro studies demonstrated that TPX2 alone promotes MT formation from purified tubulin subunits (Schatz et al., 2003; Brunet et al., 2004; Roostalu et al., 2015). Despite these advances, the molecular mechanism by which TPX2 contributes to γ-TB–dependent branching MT nucleation is currently not known.

Here, we investigate how TPX2 stimulates MT nucleation off a preexisting MT. We established the domain organization of *Xenopus laevis* TPX2 using secondary structure analysis, based on which we defined the minimal TPX2 fragment that stimulates branching MT nucleation in *Xenopus* egg extract. We found that several domains of TPX2 contribute to its ability to bind and bundle MTs, which is necessary, but not sufficient, for its aforementioned activity. Interestingly, the minimal active TPX2 fragment does not induce MT assembly in vitro, suggesting that this previously described function of TPX2 is not required for branching MT nucleation. Instead, we identified γ-TuRC nucleation activator motifs within the minimal TPX2 fragment, which are necessary for TPX2 to induce branching MT nucleation. In single-site separation-of-function mutants, binding of TPX2 to γ-TuRC remains intact whereas MT nucleation is abolished, opening the possibility that TPX2 activates γ-TuRC to promote branching MT nucleation.

Results

Domain organization of *X. laevis* TPX2

Little is known about TPX2's secondary structure, which may give insight into its function. To determine how TPX2 stimulates branching MT nucleation, we conducted secondary structure analysis and defined TPX2's domain organization. Besides using stand-alone secondary structure prediction algorithms, the most powerful prediction was obtained via the algorithm Jpred (Drozdetskiy et al., 2015), because it uses multiple sequence alignment to identify conserved secondary structure elements. The N-terminal half (amino acids 1–318), which is not required for branching MT nucleation (Petry et al., 2013), consists of a long and short α-helical region (α1 and α2). The longer C-terminal half (amino acids 319–716), which can replace endogenous TPX2 in branching MT nucleation (Petry et al., 2013), can be divided into five clusters of conserved residues separated by unstructured regions (α3–α7; Figs. 1 A and S1). The four regions α3, α4, α5, and α6 share similarity with each other in that they contain a central α-helical region that is immediately followed by a characteristic motif "FKARP" (Fig. 1, A and B; and Fig. S1). The C-terminal region (α7) is longer and mostly consists of a long α-helical stretch predicted to form a coiled coil (Figs. 1 A and S1). Based on these bioinformatics analyses, we defined these clusters as domains and designed four constructs with sequential domain deletions from the N-terminal and C-terminal end, respectively. All domain deletion constructs were expressed and purified. To experimentally verify the secondary structure prediction, we performed circular dichroism (CD) spectroscopy. The four regions that share similarity with each other display significant α-helical content but low β-sheet contribution when tested individually and in pairs (α3, α3–α4, and α5–α6), similar to the most C-terminal region (α7; Fig. 1 C). The complete C-terminal half of TPX2 (α3–α7) and a smaller fragment (α5–α7) also reflect the α-helical portion predicted (Fig. 1 C). Based on secondary structure prediction and the experimental validation using CD spectroscopy, it can be concluded that TPX2's C-terminal half consists of five domains (Fig. 1 A).

Minimal TPX2 version that stimulates branching MT nucleation

Having defined five domains that characterize the C-terminal half of TPX2, we tested for their ability to stimulate branching MT nucleation in *Xenopus* egg extract, which was visualized by total internal reflection (TIRF) microscopy. In this assay, *Xenopus* egg extract is supplemented with Alexa Fluor 568–tubulin to mark MTs and GFP-labeled end-binding protein 1 (EB1) to highlight growing MT plus ends, as well as vanadate to inhibit dynein-mediated MT gliding (Petry et al., 2013). In this condition and upon further addition of control buffer, single MTs rarely form (Fig. 1 D). In contrast, addition of the complete C-terminal TPX2 half (α3–α7) in control buffer induced the formation of hundreds of MTs within 5 min via branching MT nucleation, thus generating branched, fan-like MT structures (Fig. 1 I). Addition of TPX2 versions missing one or more domains from the C-terminal end (α3, α3–α4, α3–α5, and α3–α6) lost the ability to stimulate branching MT nucleation (Fig. 1, E–H). In contrast, domains α3 and α4 could be removed from tne N terminus to generate a TPX2 fragment that retains the ability to induce this reaction (Fig. 1, J and K). However, further deleting domains α5 and α6 abolished branching MT nucleation (Fig. 1, L and M). Together, these experiments define the construct consisting of domains α5–α7 as the minimal TPX2 version that induces branching MT nucleation (Video 1).

To quantify the nucleation kinetics of these reactions, the number of MTs was determined over time (Fig. 1, N and O). This was achieved by counting the total number of EB1-GFP comets, which mark individual MTs in our assay. Similar to control buffer, the inactive constructs display no effect on MT nucleation, whereas the active TPX2 versions clearly induce an exponential increase of MT number over time, which is typical for the mechanism of branching MT nucleation (Fig. 1 N). Averaging the kinetics of two experiments with the active TPX2 constructs α3–α7, α4–α7, and α5–α7 highlights that domains α3 and α4 are not essential for branching MT nucleation but contribute to the efficiency of this reaction by inducing it at marginally earlier time points and with a faster rate (Fig. 1 O). Similarly, although the N-terminal half of TPX2 cannot replace endogenous TPX2 (Petry et al., 2013), it seems to further increase the efficiency of this reaction compared with the C-terminal half only (Fig. S2, A–C). For all TPX2 fragments added, no significant change in MT growth speed was observed (buffer, 10.72 ± 2.28 µm/min; α3–α7, 13.12 ± 3.17 µm/min; α5–α7, 12.74 ± 3.44 µm/min; α6–α7, 11.54 ± 2.56 µm/min; α3–α6, 9.84 ± 2.15 µm/min; α3–α5, 12.34 ± 2.77 µm/min; α3–α4, 12.40 ± 2.78 µm/min).

Next, we tested whether TPX2 α5–α7 can replace endogenous TPX2. Endogenous TPX2 is sequestered by importins and therefore cannot induce branching MT nucleation in the absence of Ran-GTP. We performed an immunodepletion with TPX2 antibodies to remove endogenous TPX2 from *Xenopus* egg extract and with IgG antibodies as a control (Fig. S2 A). Upon addition of TPX2 α5–α7 to these extracts, the MT networks that formed in the presence and absence of endogenous TPX2 were indistinguishable (Fig. S2, D and E). The loss of endogenous TPX2 activity was confirmed with the addition of RanQ69L, a dominant active version of the GTPase Ran, which

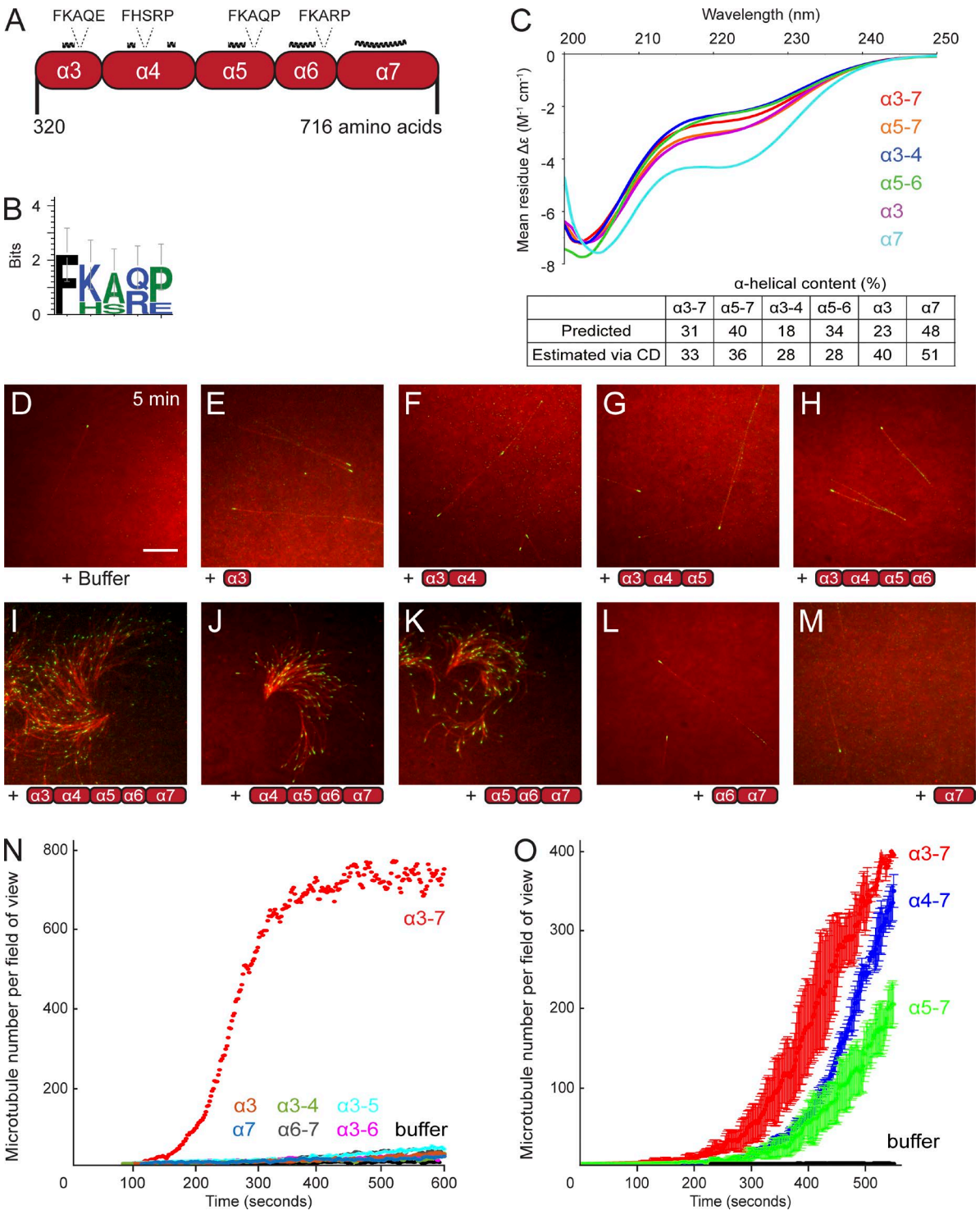

	α3-7	α5-7	α3-4	α5-6	α3	α7
Predicted	31	40	18	34	23	48
Estimated via CD	33	36	28	28	40	51

Figure 1. **TPX2 α5–α7 is the minimal construct that stimulates branching MT nucleation.** (A) Domain organization of the C-terminal half of *X. laevis* TPX2 based on secondary structure prediction using Jpred. (B) Graphical representation of the FKARP motif, which occurs after predicted α-helices in domains α3 through α6. (C) CD spectra of various TPX2 constructs in the region of 200–250 nm. All spectra suggest the presence of significant α-helical content, which is characterized by two minima near 208 nm and 220 nm. Estimates of secondary structure content using the K2D3 method agree with values obtained from the Jpred prediction. (D–M) Branching MT nucleation in *Xenopus* egg extracts in the presence of 2 µM of different truncated TPX2 constructs. The same results were obtained with a lower TPX2 concentration of 0.75 µM. EB1-GFP (green) and Alexa Fluor 568–labeled porcine brain tubulin (red) were added to the extract to follow MT plus ends and MTs, respectively. Vanadate was added to prevent dynein-mediated gliding of MTs. All images were taken after 5 min. Brightness and contrast were adjusted for each image individually to optimize visual comparison of MT structures. Bar, 10 µm. See Video 1. (N) The number of individual MTs was counted for each time frame and then plotted against time. The data are displayed for addition of TPX2 α3–α7 and all the inactive constructs. (O) Same as N, except the number of MTs is averaged over two experimental replicates for the addition of TPX2 α3–α7 and the other active constructs α4–α7 and α5–α7. Error bars represent absolute error. All extract experiments were performed at least three different times.

releases TPX2 and other spindle assembly factors (Fig. S2 E). In contrast, a TPX2 immunodepletion and addition of a fragment that cannot replace endogenous TPX2, both in the presence and absence of RanQ69L, result in few, single MTs that no longer branch (Petry et al., 2013). Thus, the minimal functional TPX2 version α5–α7 can replace endogenous TPX2 to stimulate branching MT nucleation. These experiments further validate that TPX2 addition to wild-type extract is sufficient to test the activity of the generated TPX2 constructs.

To assess whether the individual domains of TPX2 α5–α7 have a specific effect on branching MT nucleation, domains α5, α6, and α56 were individually cloned, expressed, purified, and tested in the extract addition assay. None of the individual domains or domain pairs had a noticeable effect on MT formation (Fig. S2, H–J), similar to TPX2 α6–α7 and α7 (Fig. 1, L and M). Therefore, the combination of TPX2 domains α5, α6, and α7 is necessary to induce branching MT nucleation.

Given the similarity between the four shorter α-helical domains α3, α4, α5, and α6, we addressed whether they can replace each other within TPX2 α5–α7 without loss of function. However, TPX2 domains α3 and α4 could not be swapped for α5 and α6 (TPX2 α347 in Fig. S2 M). Furthermore, neither domain α5 nor α6 could individually be replaced by domain α3 (TPX2 α367 in Fig. S2 N and α537 in Fig. S2 O). In summary, TPX2 α5–α7 is the minimal fragment that is sufficient to replace endogenous TPX2 to induce branching MT nucleation.

Finally, we tested whether TPX2 stimulates the formation of any MT or only MTs originating from preexisting ones. For this purpose, augmin was immunodepleted from *Xenopus* egg extract using an antibody specific against the Haus 1 subunit (Fig. S3 A). The level of augmin depletion was very high (Haus 1, 92 ± 3%), whereas codepletion of γ-TuRC remained low (γ-tubulin, 20 ± 14%; GCP5, 9 ± 3%; Fig. S3 B). Direct immunodepletion of γ-tubulin from *Xenopus* egg extract virtually abolishes all MT nucleation, whereas immunodepletion of augmin allows for the formation of few single MTs but prevents branching MT nucleation (Petry et al., 2013). This effect is not caused by the partial codepletion of γ-tubulin (Petry et al., 2011). In this Haus 1–depleted extract, neither the addition of TPX2's C-terminal half nor the addition of full-length TPX2 had any discernable effect, whereas addition of TPX2's C-terminal half to the control immunodepletion led to branched, fanlike MT structures (Fig. S3, C and E). The same results were obtained when these TPX2 additions were done in the presence of RanQ69L (Fig. S3, D and F). Collectively, these results suggest that irrespective of other spindle assembly factors released by RanGTP, TPX2 acts together with augmin to promote branching MT nucleation in *Xenopus* egg extract.

Functional characterization of truncated TPX2 constructs in vitro

Having identified several TPX2 domain constructs that retained MT nucleation activity whereas others did not, we asked what might be responsible for this difference. It was previously observed that the active C-terminal half of TPX2 (319–716), but not the inactive N-terminal half (1–480), localizes to branched MT structures in *Xenopus* egg extract (Petry et al., 2013). This C-terminal half of TPX2 was observed to bind along all MTs without any preference. Based on these findings we hypothesized that MT binding might be important for TPX2 function in MT-dependent MT nucleation. To determine whether loss of MT binding is responsible for the loss of nucleation activity of the inactive truncated TPX2 constructs, we measured the ability of these proteins to bind MTs in an in vitro co-sedimentation assay. The complete C-terminal half, TPX2 α3–α7, displayed strong binding to MTs in vitro (Fig. 2 A). Over half of the MT binding activity was retained in TPX2 constructs that contained three or four domains, such as TPX2 α5–α7, TPX2 α3–α6, and TPX2 α3–α5 (Fig. 2 A). In contrast, TPX2 versions that contained only two domains, such α3–α4, α5–α6, and α6–α7, bound very poorly (∼10-fold less) to MTs in vitro (Fig. 2 A). Furthermore, single domains like α6 and α7 barely showed MT-binding activity (Fig. 2 A). Because the MT-binding capacity does not rise linearly with the addition of a domain, multiple domains must cooperatively mediate MT binding. These results suggest that at least three successive domains, irrespective or their identity, are necessary for significant MT binding in vitro.

TPX2 has been characterized as a MT-bundling protein (Schatz et al., 2003). We hypothesized that this could be of particular importance for branching MT nucleation, because ∼43% of newly nucleated MTs grow parallel (i.e., at a 0-degree angle) to the mother MT (Petry et al., 2013), which likely requires MT bundling activity either between both MTs or at the branch point. Therefore, we assessed the ability of these truncated TPX2 constructs to bundle preformed MTs (Fig. 2 B). MT bundling activity increased with the number of consecutive TPX2 domains (Fig. 2 B), displaying the same trend observed in the MT-binding experiments.

In summary, there is not one single MT-binding or bundling domain within the C-terminal half of TPX2. Instead, a minimum of three successive domains are necessary to display significant MT-binding and bundling activity. However, several of the TPX2 fragments, such as α3–α6 and α3–α5, bind and bundle MTs yet are inactive in MT-dependent MT nucleation. This implies that MT binding and bundling are not sufficient to define TPX2 constructs that actively induce branching MT nucleation.

Besides MT binding and bundling, multimerization could be an important property of TPX2 in branching MT nucleation. To test whether *X. laevis* TPX2 exists in a monomeric or multimeric form in solution, the protein was assessed by size exclusion chromatography coupled with multiple angle light scattering (SEC-MALS). Both the complete C-terminal half (α3–α7) and the minimal fragment TPX2 α5–α7 exist as monomers in solution (Fig. S4, A and B). Next, we hypothesized that TPX2 binding to α/β-tubulin heterodimers could be necessary to induce branching MT nucleation. However, neither TPX2 α3–α7 nor α5–α7 bound to unpolymerized tubulin as tested by SEC (Fig. S4 C).

Several motifs within TPX2 α5–α7 are necessary for branching MT nucleation

To determine what sets the active TPX2 α5–α7 apart from the remainder of the protein, we analyzed its amino acid sequence and discovered several conserved regions that share sequence similarity with the two γ-TuRC nucleation activator motifs discovered so far: SPM and γTuNA (Fig. 3, A and B). The SPM-like motif resides within domain α5 (Fig. 3, A and B). The γTuNA-like motif also begins within domain α5 and partly overlaps with the SPM-like motif (Fig. 3, A and B). Interestingly, the γTuNA-like motif is not consecutive in TPX2 but separated by an unstructured region of 30 amino acids (Fig. 3 B; amino acids 532–561). This places the second half of γTuNA into domain α6 (Fig. 3, A and B). The SPM and the first part of the γTuNA motif, which we denote γTuNAa, make up the α-helical region

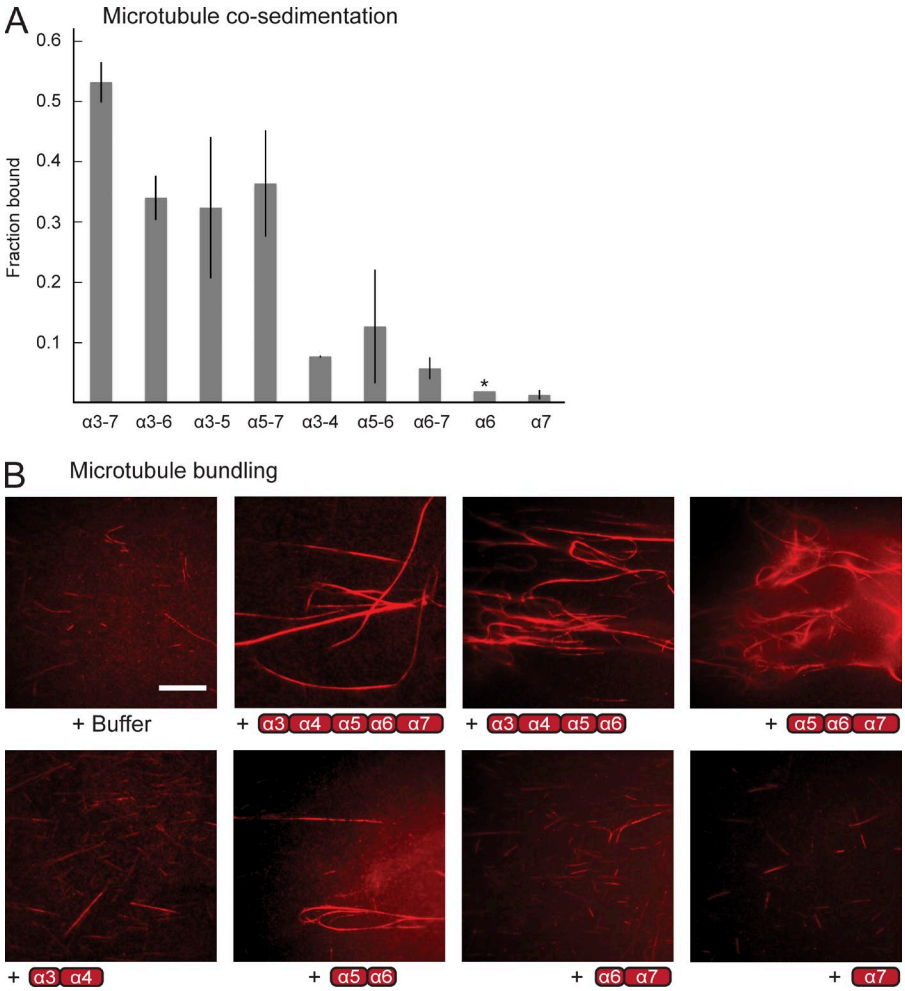

Figure 2. **Multiple domains of TPX2 contribute to its ability to bind and bundle MTs in vitro.** (A) Co-sedimentation assay of 1 µM of various TPX2 constructs with Taxol-stabilized MTs in vitro. The ratio of protein in the supernatant and pellet after centrifugation was used to calculate the fraction of total protein bound to MTs. Values are the mean of two experiments, and error bars represent standard deviation. *, TPX2 α6 was only tested once. (B) MT bundling assay using Alexa Fluor 568–labeled GMPCPP-stabilized MTs in vitro with 1 µM of various TPX2 constructs. Bar, 10 µm. Assay was repeated three times.

within domain α5 (Figs. 3 A and S1). In contrast, the second part of the γTuNA motif, which we call γTuNAb, precedes α-helical region α6 (Figs. 3 A and S1). The most conserved stretch of overlap between SPM and γTuNAa motifs (LQKEKRLDE LRKD) can be found in at least one other, currently unnamed protein of the *X. laevis* proteome (Kwon et al., 2014), implying confidence that this motif combination is conserved and may play an important role.

We addressed whether these regions are important for MT nucleation activity by deleting them to generate TPX2 α5–α7 ΔSPM, ΔγTuNAa, and ΔγTuNAb. These TPX2 versions were expressed, purified and tested for their ability to induce branching MT nucleation. Surprisingly, none of the three constructs stimulated MT nucleation (Fig. 4, E–G). This is reflected in the kinetics, in which TPX2 α5–α7 induces an exponential increase of MT number over time, whereas the three deletion constructs barely generated individual MTs similar to the control (Fig. 4 J). Yet, all three inactive TPX2 versions retained their ability to bind to MTs in vitro (Fig. S5 A), implying that the inability to stimulate branching MT nucleation is not caused by loss of MT binding or improper folding of the deletion constructs.

Besides these newly discovered motifs, several other regions of TPX2 that reside in the fragment α5–α7 have been previously described. A seven-amino-acid sequence preceding α-helical region α7 is present in *X. laevis* TPX2 but absent in its *Xenopus tropicalis* homologue. This absence has been shown to render TPX2 more active by forming more MT asters in *X. laevis* egg extract (Helmke and Heald, 2014). We generated a *X. laevis* TPX2 α5–α7 Δtrop protein, which is missing these seven amino acids, and tested its effect on branching MT nucleation. TPX2 α5–α7 Δtrop stimulates branching MT nucleation more strongly by increasing the rate of nucleation upon its addition (Fig. 4 H, K). This is consistent with its effect on spindle formation (Helmke and Heald, 2014) and shows that changes in the amino acid sequence of TPX2 can also lead to an increase in its activity to stimulate branching MT nucleation.

The C-terminal amino acids of TPX2 are responsible for interacting with the tetrameric kinesin Eg5 (Eckerdt et al., 2008; Ma et al., 2010). To test whether this region is important for branching MT nucleation, it was deleted from TPX2 α3–α7. Unexpectedly, the resulting TPX2 α3–α7 ΔEg5 did not stimulate branching MT nucleation when added to *Xenopus* egg extract (Fig. 4, C and I). This loss of function is independent of its retained activity to bind to MTs (Fig. S5 A). Furthermore, this is not caused by a loss of Eg5 motor activity because inhibition of Eg5 via the drug STLC has no discernable effect on branching MT nucleation (unpublished data). In summary, we defined five motifs, which reside in the minimal active construct TPX2 α5–α7 and have an important role in branching MT nucleation.

To further test the functional importance of these motifs, we introduced single-site mutations at selected positions within TPX2 α5–α7. Conserved phenylalanine (Phe) residues were replaced with an AzidoPhe moiety, which was incorpo-

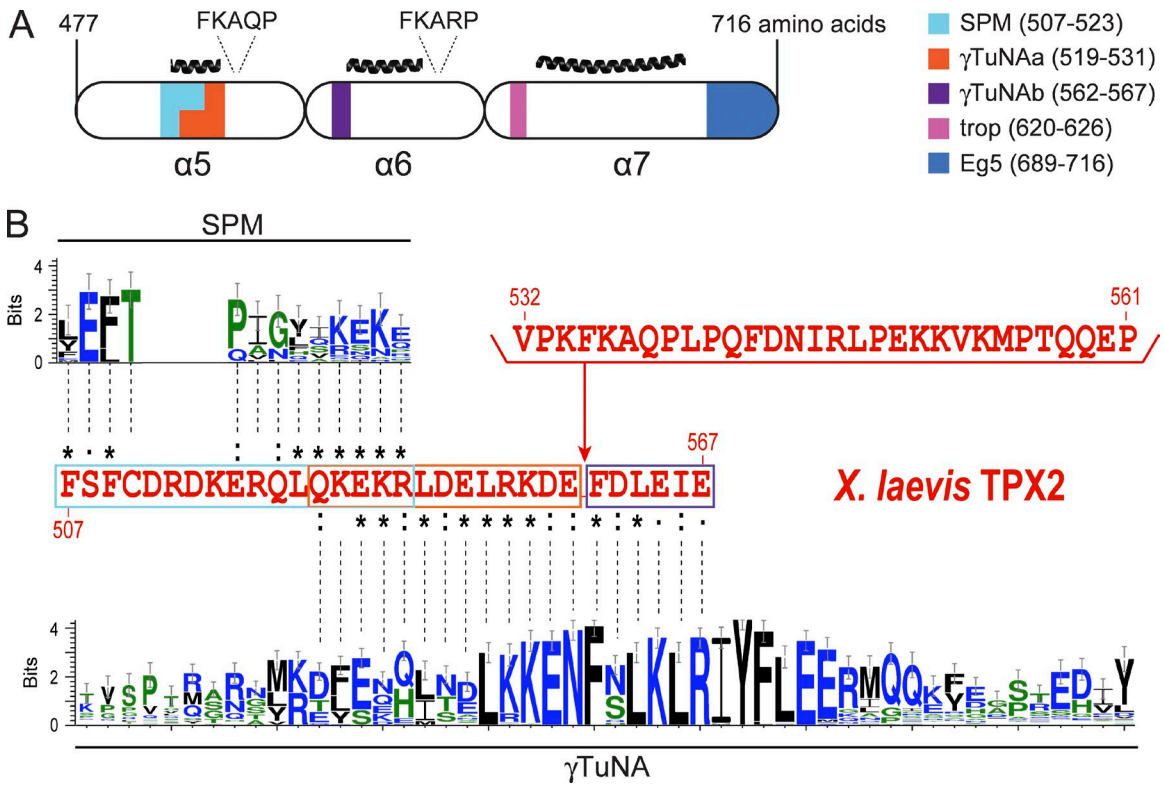

Figure 3. **Identification of novel motifs within TPX2 α5–α7.** (A) Domain organization of TPX2 α5–α7 showing newly found motifs. Amino acids 507–523 (cyan) share homology with the SPM, and amino acids 519–531 (orange) and 562–567 (purple) share homology with the γTuNA motif, both of which have a γ-TuRC activation function in the proteins where they were originally identified. Amino acids 620–626 (pink) have been suggested to negatively regulate MT nucleation in *Xenopus* egg extract, and their absence in *X. tropicalis* TPX2 leads to increased MT formation. Amino acids 689–716 (blue) are necessary for the interaction between TPX2 and the kinesin Eg5. (B) Graphical representation of the SPM of pericentrin/Spc110 across multiple species and the γTuNA motif of Mto1/centrosomin/CDK5RAP2 and the related myomegalin across multiple species. The motif sequence logos were made using WebLogo 3. Sequence alignment reveals homology between these motifs and sequences within TPX2 α5–α7 (red sequence), revealing the new motifs SPM (cyan box), γTuNAa (orange box), and γTuNAb (purple box). γTuNAa and γTuNAb are separated by a stretch of 29 amino acids.

rated via a suppressor tRNA that reads the TAG stop codon. The purified proteins were then tested in the branching MT nucleation assay. TPX2 α5–α7 with a single-site mutation in a region without any functional or secondary structure motif (F492AzF), and one following the seven amino acids stretch that is missing in *X. tropicalis* (F629AzF), each displayed similar activity as the wild-type version (Fig. 5, C, D, I, and N). A single-site mutation at the very C terminus (F714AzF) retained activity at an intermediate level (Fig. 5, L and N). In contrast, replacement of Phe within the SPM (F507AzF) and the γTuNAb motif (F562AzF) inactivated TPX2 α5–α7 (Fig. 5, E, G, and M). Interestingly, single-site mutations following the FKARP motif of domain α5 (F543AzF) and within the FKA RP motif of domain α6 (F594AzF) caused the complete loss of activity (Fig. 5, F, H, and M), suggesting that these motifs are essential for stimulating branching MT nucleation activity as well. Replacing Phe within the long α-helical region of domain α7 (F643AzF) and the C-terminal residues of the unstructured region that interacts with Eg5 (F710AzF) also rendered TPX2 inactive (Fig. 5, J, K, and M), confirming that both the unstructured C terminus and the long α-helical stretch of domain α7 are functionally important.

The incorporation of AzF was chosen to site-specifically cross-link the various identified motifs of TPX2 with γ-TuRC and thereby reveal their exact binding sites; however, this approach was not successful because of a limiting yield for mass spectrometry analysis. At the same time, all single-site mutants retained the ability to bind MTs as assessed in a MT co-sedimentation assay (Fig. S5 B). This confirms that each TPX2 construct is folded and retains an independent function. MT binding thus remains necessary but is not sufficient in TPX2 to stimulate branching MT nucleation. In summary, not only the γ-TuRC nucleation activator motifs and the C-terminal end but also the FKARP repeats of domains α5 and α6 and the C-terminal α-helical region are critical for branching MT nucleation.

TPX2 α5–α7 does not possess intrinsic MT nucleation activity

A hallmark of TPX2 has been its intrinsic MT nucleation activity independent of any other protein (Schatz et al., 2003; Brunet et al., 2004; Roostalu et al., 2015). To test whether this could be relevant for TPX2's mechanism of stimulating branching MT nucleation, we performed MT nucleation assays with purified TPX2 constructs and tubulin. Only a few MTs assembled in the absence of TPX2 (Fig. 6 A). As previously described, full-length TPX2 is able to nucleate MTs on its own (Fig. 6 A) and forms tubulin aggregates at higher tubulin concentrations from which MTs emanate, reminiscent of MT asters (Fig. 6 B; Schatz et al., 2003; Brunet et al., 2004). Similarly, the C-terminal half of TPX2 forms tubulin aggregates and nucleates MTs, albeit to a lesser extent (Fig. 6, A and B; Schatz et al., 2003; Brunet et al., 2004). Surprisingly, the minimal construct that activates branching MT nucleation,

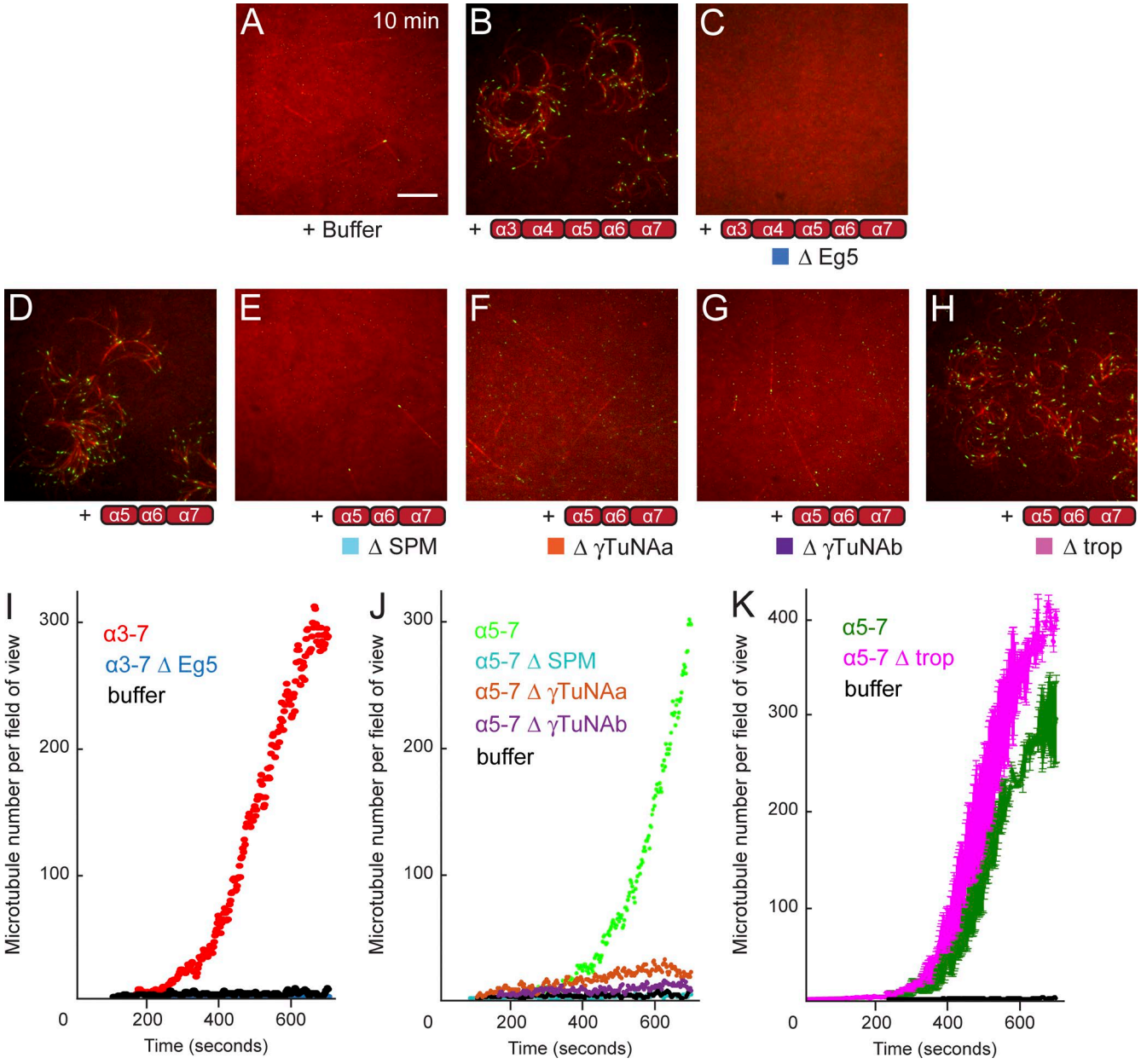

Figure 4. **The newly identified motifs in TPX2 are necessary to stimulate branching MT nucleation.** (A–H) Branching MT nucleation in *Xenopus* egg extracts and in the presence of 2 µM TPX2 α3–α7 or α5–α7, with and without various motif deletions. The same results were obtained with a lower TPX2 concentration of 0.75 µM. EB1-GFP (green) and Alexa Fluor 568–labeled porcine brain tubulin (red) were added to follow MT plus ends and MTs, respectively. Vanadate was added to prevent dynein-mediated gliding of MTs. All images were taken after 10 min. Brightness and contrast were adjusted for each image individually to optimize visual comparison of MT structures. Bar, 10 µm. See Video 2. (I and J) For each reaction, the number of individual MTs was counted for each time frame and then plotted against time. The data are displayed for TPX2 α3–α7 and TPX2 α5–α7 and their inactive deletion mutants. (K) Same as I and J, but here the number of MTs is averaged over two experimental replicates for TPX2 α5–α7 and the only active deletion mutant, TPX2 α5–α7 Δtrop. Error bars represent absolute error. All extract experiments were performed at least three different times.

TPX2 α5–α7, has no MT nucleation activity on its own (Fig. 6, A and B). This implies that the intrinsic MT nucleation activity of TPX2 is not required for branching MT nucleation and that TPX2 acts through another molecular player to promote MT nucleation in *Xenopus* egg extract.

Binding to γ-TuRC is unaffected in TPX2 α5–α7 and its single-site mutants

The TPX2 fragments with single-site mutations might no longer be functional because they lost their ability to either activate γ-TuRC or bind to γ-TuRC. To address these two possibilities, we tested whether GFP-tagged TPX2 constructs coupled to anti-GFP beads can still bind to γ-TuRC from *X. laevis* egg extract. Although GFP alone was not able to coimmunoprecipitate γ-TuRC, TPX2 α5–α7 displays binding to γ-TuRC components (Fig. 7). Surprisingly, all single-site mutants, independent of whether they are functional or not, bound γ-TuRC in the immunoprecipitation assay in an indistinguishable manner. This indicates that the binding to γ-TuRC is not affected and not the reason for the loss of MT nucleation activity. Rather, all TPX2 versions can still bind to γ-TuRC but some can

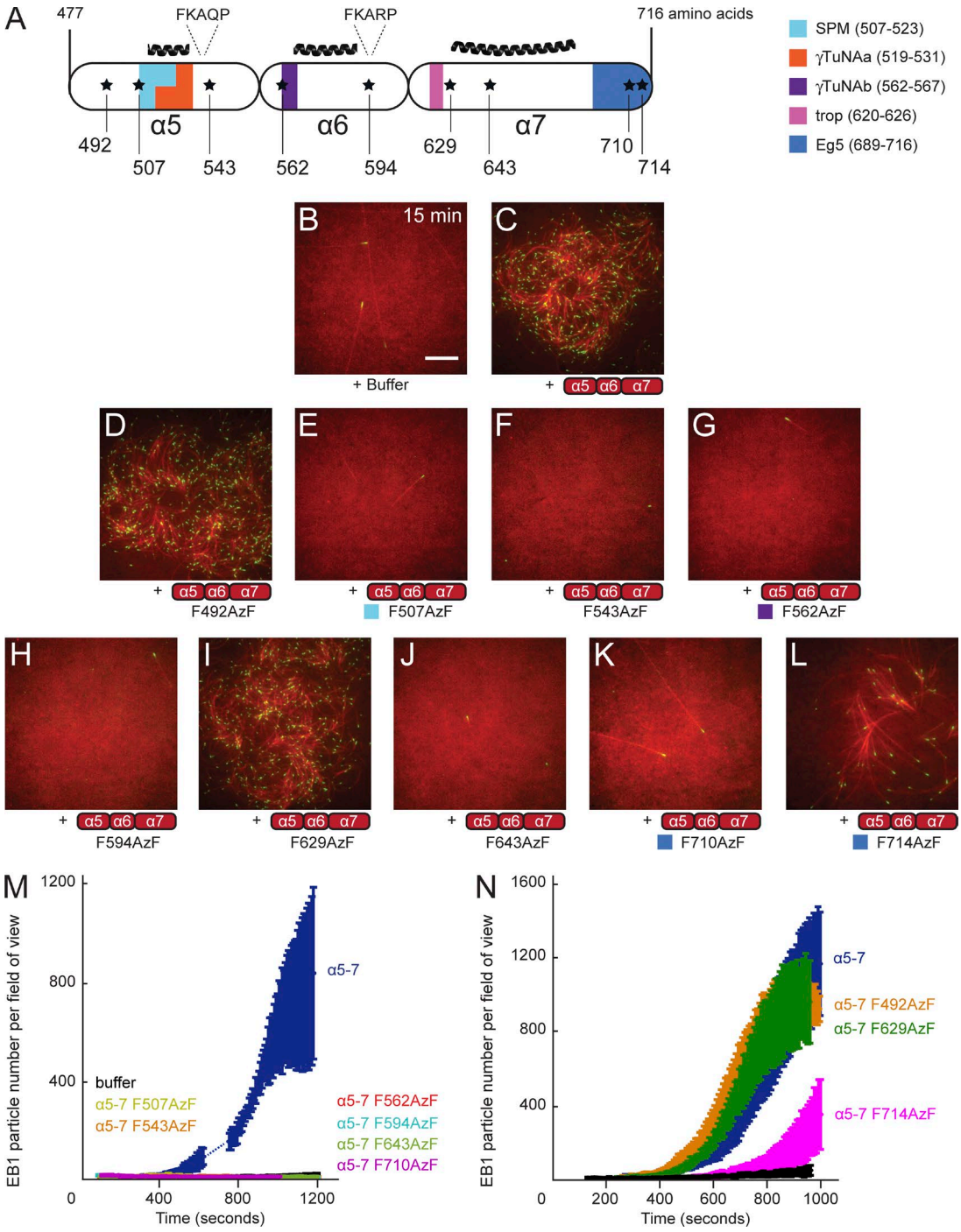

Figure 5. **Branching MT nucleation activity of multiple TPX2 single-site mutants.** (A) Domain organization of TPX2 α5–α7 showing the location of single-site mutations. (B–L) Branching MT nucleation in *Xenopus* egg meiotic extracts and in the presence of 2 µM TPX2 α5–α7 with and without various single-site mutations. The same results were obtained with a lower TPX2 concentration of 1 µM. Images for F492AzF, F629AzF, and F714AzF mutants, which show a high level of activity, as well as the image for the positive control TPX2 α5–α7, were collected using one extract. Images for the rest of the mutants and the negative control were collected with a different extract. This was necessary because the lifetime of one extract was incompatible with the high number of samples; however, both controls are representative and consistent among all extracts tested. EB1-mCherry (green) and Cy5-labeled porcine brain tubulin (red) were added to the extract to follow MT plus ends and MTs, respectively. Vanadate was added to prevent dynein-mediated MT gliding. All images were acquired after 15 min. Brightness and contrast were adjusted for each image individually to optimize visual comparison of MT structures. Bar, 10 µm. See Video 3. (M) The number of EB1 particles was counted for three different fields of view and the mean was plotted against time. The data are displayed for the addition of TPX2 α5–α7 and all the inactive mutants. Data collection for the positive control, TPX2 α5–α7, was interrupted in the region denoted by the dashed line. Error bars represent standard deviation. (N) Same as M, but the data are depicted for the addition of TPX2 α5–α7 and mutants that have full or intermediate activity. Measurements also represent the mean of three different fields of view, and the error bars denote standard deviation. All extract experiments were performed at least three different times.

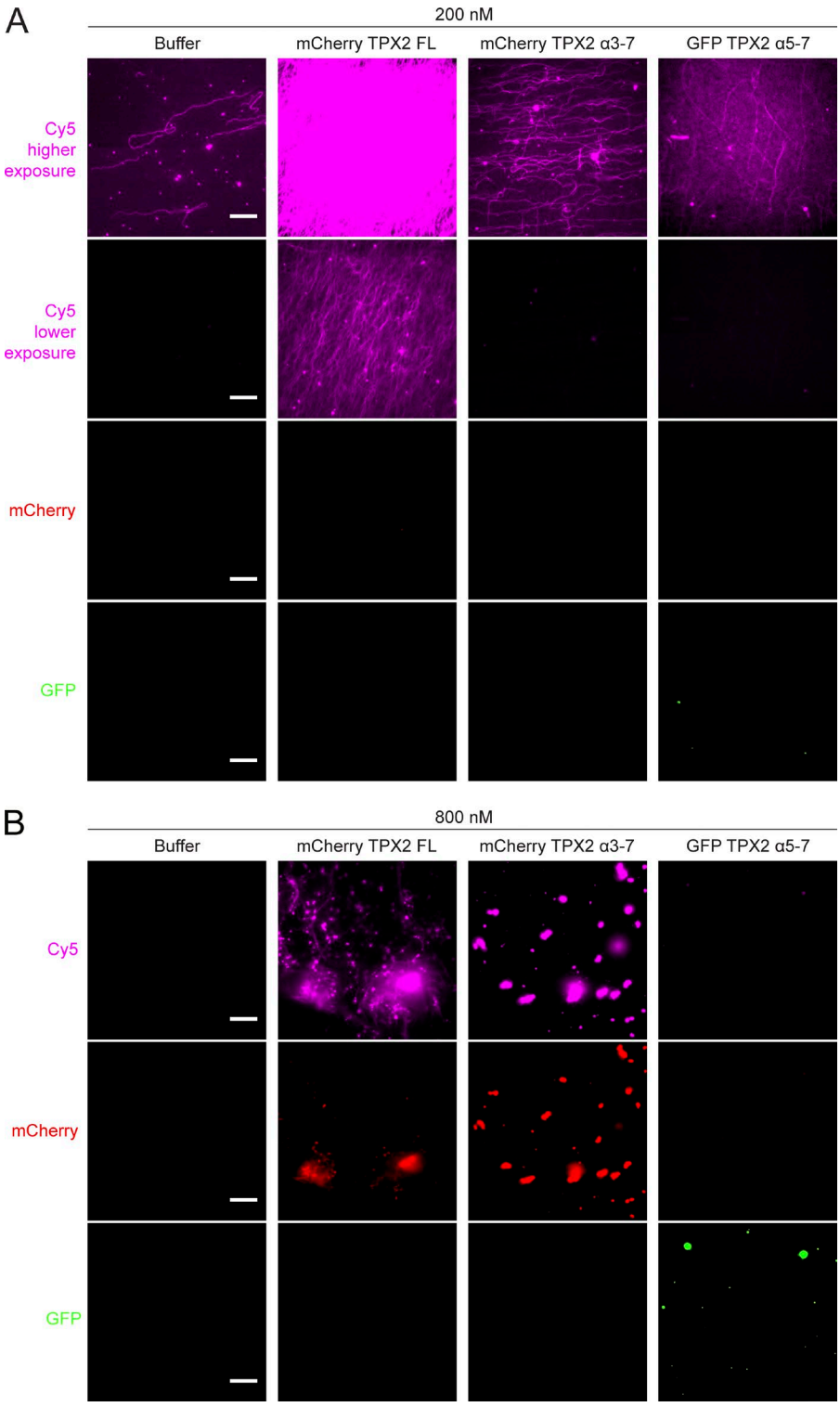

Figure 6. **TPX2 α5–α7 does not induce MT assembly in vitro.** (A) Representative images of MTs formed after incubation of 200 nM fluorescent full-length TPX2, TPX2 α3–α7, and TPX2 α5–α7 with 30 µM tubulin. (B) Same as A, but using 800 nM of each TPX2 construct. At this concentration, full-length TPX2 and TPX2 α3–α7 also form tubulin aggregates. Assay was repeated two times. Bars, 10 µm.

no longer activate it for branching MT nucleation. In contrast, no binding of TPX2 α5–α7 to augmin could be detected by immunoprecipitation experiments (Fig. S5 C). Furthermore, immunoprecipitation of endogenous TPX2 from *Xenopus* egg extract shows that full-length TPX2, similar to TPX2 α5–α7, lacks a robust interaction with augmin, but still binds to γ-TuRC, confirming this as a critical interaction (Fig. S5 D).

Discussion

Here, we established the domain organization of *X. laevis* TPX2's C-terminal half, which is sufficient to stimulate branching MT nucleation. Domain deletion constructs with and without activity still bind and bundle MTs. In contrast, the minimal active construct cannot nucleate MTs on its own, and is defined by γ-TuRC nucleation activator motifs. When these motifs are

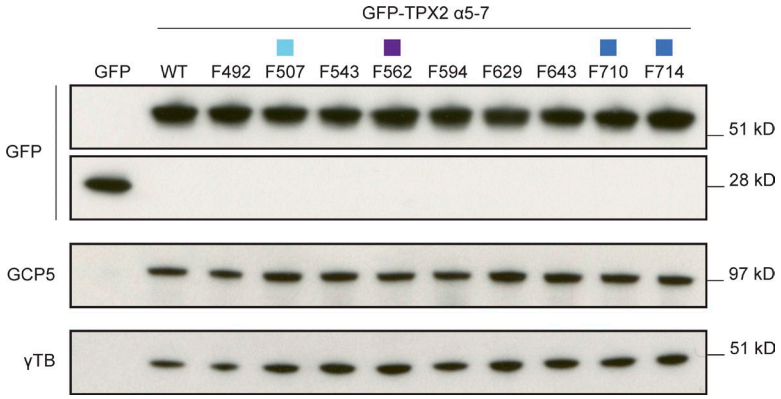

Figure 7. **Single-site mutations within TPX2 α5–α7 do not interfere with the interaction of γ-TuRC.** Immunoprecipitation of 1 µM GFP-tagged TPX2 constructs from *Xenopus* egg extracts using an antibody specific against GFP. The same GFP antibody was used for detection in the immunoblot, along with commercial antibodies against GCP5 and γ-tubulin. Assay was repeated three times. WT, wild type.

mutated, this minimal active construct retains its binding to γ-TuRC, suggesting that TPX2 might activate γ-TuRC to promote branching MT nucleation.

Domain definition of a MT nucleation effector protein

TPX2 was first described almost two decades ago (Wittmann et al., 2000), and it has been extensively studied. Many of its binding partners have been identified along with their discrete binding sites on TPX2. In the past, deletion constructs were made by cutting along the amino chain length in certain intervals (Schatz et al., 2003; Trieselmann et al., 2003; Brunet et al., 2004; Eckerdt et al., 2008). However, little was known about TPX2's secondary and tertiary structure. Here, we conducted a thorough secondary structure analysis and discovered four similar domains (α3, α4, α5, and α6), each characterized by an α helical region followed by a motif FKARP. Finally, a longer α-helical domain α7 terminates the protein. Recently, a study using CD spectroscopy estimated significant (68%) α helical content in the full-length *X. laevis* TPX2 protein, and also identified regions in the C-terminal half of TPX2 that share sequence homology with each other (Sanchez-Pulido et al., 2016). These findings support our identification of five domains in the C-terminal half of TPX2. Expressing and purifying individual domains or combinations thereof yielded folded protein, which was confirmed by CD spectroscopy and MT binding in vitro. Together, these tests validate that each defined domain indeed has the α-helical content predicted and is a folded unit of TPX2. Defining the domain organization of TPX2 is an important step toward studying their individual function and how they work. This type of analysis has been instrumental in understanding the mechanism of molecular motors (Vale and Milligan, 2000) and polymerases, such as XMAP215 (Widlund et al., 2011). We now have separated domains that are critical for TPX2 function, which to our knowledge is the first domain definition of a MT nucleation effector protein and provides a basis for studying how MT nucleation is regulated in space and time, and for future structural studies.

TPX2 is made up of functionally distinct domains

Functionally distinct domains mediate the various activities of TPX2's C-terminal half. Surprisingly, none of the single domains (α3, α4, α5, α6, or α7) display MT binding or bundling activities. In contrast, the higher the number of the joined domains, the stronger they bind to and bundle MTs. This effect does not seem to be mediated by multimerization of *X. laevis* TPX2 in solution, because it exists as a monomer, consistent with a recent study of human TPX2 (Roostalu et al., 2015). Rather multiple domains may act in a cooperative manner to provide the interface necessary to interact with one or more MT lattices. Previously published literature reported many different fragments of TPX2 to mediate binding to MTs, which somewhat contradicted each other (Schatz et al., 2003; Trieselmann et al., 2003; Brunet et al., 2004). However, these results can now be explained by the fact that at least three domains within TPX2's C-terminal half, irrespective of their identity, mediate significant MT binding. Furthermore, MT binding activity within the C-terminus of TPX2 is supported by the finding that importin α, which binds to amino acid site 284 in the N-terminal half of TPX2, has no effect on the interaction of TPX2 with MTs (Schatz et al., 2003).

The C-terminal domain α7 cannot be deleted, nor can its C-terminal tail be removed without loss of the ability to induce branching MT nucleation. The C-terminal 35 amino acids are required for the interaction with Eg5, yet Eg5 inhibition by STLC has no effect on branching MT nucleation. This could be explained if merely binding to Eg5, albeit in an inhibited state, is sufficient to induce branching MT nucleation. Alternatively, and possibly more likely, the C-terminal region may be involved in another function that remains to be identified, because STLC inhibits Eg5 movement and in many cases causes release from MTs (Balchand et al., 2015).

In addition, our finding that the deletion of the seven amino acids that are absent in *X. tropicalis* TPX2 enhance MT nucleation efficiency of *X. laevis* TPX2, supports the discovery that deleting this region increases the formation of MT asters in *Xenopus* egg extract (Helmke and Heald, 2014). Perhaps the most unexpected finding in our study is that domains α3 and α4, despite sharing similarity in the secondary structure with domains α5 and α6, are not essential to induce branching MT nucleation. Thus, the ability to induce branching MT nucleation is encoded in the minimal functional construct, TPX2 α5–α7.

γ-TuRC nucleation activation motifs in TPX2

Two types of γ-TuRC nucleation activation motifs have been discovered so far, the SPM and the γTuNA/CM1 motifs. Only the budding yeast protein Spc110, which contains both motifs, the human protein CDK5RAP2 and the fission yeast protein Mto1, which each contain a γTuNA motif only, have been characterized for their effect to activate MT nucleation in a γ-TB dependent manner (Samejima et al., 2008; Choi et al., 2010; Lin et al., 2014). Here, we found that TPX2 contains an SPM-like and a γTuNA-like motif. They are unique in that they partly

overlap with each other and an unstructured amino acid region in TPX2 separates the γTuNA-like motif. The regions we define as γTuNAa and b correspond, based on sequence alignments, to the Mto1-9A1 and Mto1-9B regions of Mto1's CM1 motif, respectively (Samejima et al., 2008). The two motif halves of Mto1 are separated by a single nonconserved amino acid, whereas the γTuNA/CM1 motif in TPX2 is separated by a long stretch of amino acids, indicating that this could be a loop region of variable size in different proteins. Interfering with the SPM and γTuNA motifs in TPX2 abrogates branching MT nucleation, whereas γ-TuRC binding remains intact, suggesting that TPX2 might act as a γ-TuRC activator. Besides containing these shared motifs, TPX2 also displays some differences to the other γ-TB complex effectors. First, when H.s. CDK5RAP2's conserved F75 residue was mutated to an alanine, the protein no longer bound to γ-TuRC, thus preventing its activation (Choi et al., 2010). The equivalent residue in *X. laevis* TPX2 is F562 and lies within its γTuNAb motif. When mutated, TPX2 can still bind to γ-TuRC, but no longer activates it for branching MT nucleation. Similarly, the CM1 region in Mto1 is also required for binding to γ-TuRC based on coimmunoprecipitation experiments (Samejima et al., 2008). Although the γTuNA/CM1 motif in CDK5RAP2 and Mto1 can also be considered to have γ-TuRC localization function (Fong et al., 2008; Samejima et al., 2008; Choi et al., 2010), TPX2's γTuNA-like motif seems to have no obvious role in γ-TuRC localization. The yeast pericentrin homologue Spc110 also contains both an SPM and a CM1 motif, but they are not overlapping and are separated by dozens of amino acids. Phosphorylation by the kinases Mps1 and Cdk1 within this separating region activate γ-TuSC oligomerization (Lin et al., 2014). It remains to be tested whether the regions within and between the SPM and γTuNA motifs in TPX2 are also regulated by posttranslation modifications.

Surprisingly, a single-site mutation within the FKARP motif of domain α6 and following the motif in domain α5 was no longer able to stimulate branching MT nucleation. This suggests that FKARP is a novel motif that also has a role in regulating MT nucleation, whereas its precise mode of action remains to be identified.

Model for how TPX2 activates branching MT nucleation

Several mechanisms could account for how TPX2 stimulates branching MT nucleation. Although discussed separately, they are not mutually exclusive and multiple mechanisms may contribute together.

In vitro, several functions have been described for TXP2, which could be relevant for a model in which TPX2 directly interacts with tubulin to induce MT nucleation. For example, TPX2 has been characterized to bind and bundle MTs, form tubulin aggregates, nucleate MTs from pure tubulin in vitro, and directly affect MT dynamics (Schatz et al., 2003; Brunet et al., 2004; Roostalu et al., 2015; Wieczorek et al., 2015; Reid et al., 2016). These features could be important for directly supporting the formation of a MT seed, which may help overcome kinetic barriers in MT nucleation. However, MT binding and bundling is necessary, but not sufficient, to induce branching MT nucleation for TPX2 fragments studied here. Second, the minimal TPX2 fragment that we characterized to retain activity (α5–α7) does not form tubulin aggregates or exhibit intrinsic MT nucleation activity, in contrast to the C-terminal half and full-length TPX2. This is in accordance with the findings that the potential of TPX2 to nucleate MTs on its own is negatively regulated when importin α is bound to site 284 in the N-terminal half (Schatz et al., 2003), and that the region of TPX2 responsible for forming MTs in vitro seems to reside in amino acids 1–480 (Brunet et al., 2004). Third, we do not see a significant change in MT growth speed upon addition of TPX2 fragments or in MT shortening, which can rarely be observed in extract. In contrast, TPX2 has a direct effect on MT dynamics in vitro (Wieczorek et al., 2015). By suppressing tubulin subunit off-rates during MT assembly and disassembly, TPX2 allows for the support of very slow rates of plus-end MT growth, which also leads to a dramatically reduced MT shortening rate (Reid et al., 2016). Because none of these described functions are retained in TPX2 α5–α7, a mechanism in which TPX2 directly influences tubulin dimers is less likely to induce MT nucleation.

One of the most surprising findings in this study is that TPX2 contains SPM- and γTuNA-like motifs that are functionally important. Single-site mutations introduced in these motifs still allow binding to γ-TuRC but no longer stimulate branching MT nucleation. These findings support a mechanism in which TPX2 directly activates γ-TuRC. However, our results do not rule out the possibility that the minimal TPX2 fragment could recruit an additional factor from the extract to promote branching MT nucleation. In addition, the effect of TPX2 on MT nucleation requires augmin, a factor that so far has been characterized to recruit γ-tubulin to preexisting MTs (Goshima et al., 2008; Lawo et al., 2009; Uehara et al., 2009). To ultimately test the concrete role and mechanism of augmin and to directly demonstrate that TPX2 activates γ-TuRC in branching MT nucleation, it will be necessary to reconstitute this reaction from purified components in vitro in the future.

Although the N-terminal half of TPX2 cannot replace endogenous TPX2 to induce branching MT nucleation (Petry et al., 2013), full-length TPX2 containing this N-terminal half is more efficient than its C-terminal half in stimulating branching MT nucleation, as shown here. The N-terminal half of TPX2 is important to facilitate MT nucleation from pure tubulin in vitro (Schatz et al., 2003; Brunet et al., 2004; Roostalu et al., 2015). In addition, the N-terminal half of TPX2 harbors binding sites for Aurora A kinase and importin α, which regulate TPX2's activity (Kufer et al., 2002; Schatz et al., 2003; Tsai et al., 2003; Scrofani et al., 2015). Thus, these two features of the N-terminal half (i.e., the intrinsic MT nucleation activity and regulation via other factors) may contribute to the increased efficiency of full-length TPX2 to stimulate branching MT nucleation. Nevertheless, it is clarified here that the effect of TPX2 on MT nucleation in *Xenopus* egg extract is augmin dependent, suggesting that TPX2 only promotes MT nucleation from preexisting MTs. Most importantly, TPX2 now provides a direct link between RanGTP, which is activated in the vicinity of chromatin, and γ-TuRC, which mediates MT formation throughout the mitotic spindle.

Materials and methods

Sequence analysis

The primary sequence of the *X. laevis* TPX2 protein was subjected to secondary structure prediction combined with homology analysis using the Jpred online tool (Drozdetskiy et al., 2015). Clustal Omega (Sievers et al., 2011) was used for multiple sequence alignment of TPX2 α5–α7 with the γTuNA motif of Mto1/centrosomin/CDK5RAP2/myomegalin

and the SPM motif of pericentrin/Spc110. The actual motif sequences used were described for multiple orthologues from yeast to human (Fong et al., 2008; Lin et al., 2014). The WebLogo 3 online tool (Crooks et al., 2004) was used to graphically represent the relative frequency of each amino acid at each position of the SPM and γTuNA motifs.

Plasmid construction

X. laevis TPX2 α3–α7 (amino acids 320–716) was cloned via SalI and NotI sites into the pGEX4T1 expression vector with an N-terminal GST tag. C-terminally truncated constructs were made by incorporating a STOP codon at the desired position via site-directed mutagenesis. N-terminally truncated fragments and fragments truncated from both termini were PCR-amplified and inserted into pGEX4T1 via SalI and NotI sites. TPX2 constructs with swapped domains (α3–α4–α7, α3–α6–α7, and α5–α3–α7) were synthesized (Genscript) and cloned into the pGEX4T1 vector. Site-directed mutagenesis (New England Biolabs, Inc. and Agilent Technologies) was used to make TPX2 constructs with deleted motifs and with single-site mutations, in which the codon of Phe was changed to the TAG stop codon. The single-site mutants were inserted into the vector GT-RAA-H with N-terminal msfGFP and TEV tags and a C-terminal His6 tag. Fluorescently labeled TPX2 α3, α3–α4, α7, and α5–α7 were made by PCR amplification and insertion into 9GFP vector (Macrolab) with an N-terminal His6-GFP tag. Fluorescently labeled TPX2 α3–α7 and α5–α6 were made by PCR amplification and insertion into 9GFP (Macrolab) with an N-terminal His6-mCherry-tag vector (HC-RAA). Full-length mCherry-TPX2 was constructed by PCR-amplification and simultaneous ligation of mCherry and TPX2 into the pST50Tr-STRHISNDHFR vector (Tan et al., 2005) using Gibson Assembly (New England Biolabs, Inc.). All constructs were fully sequenced. Table S1 summarizes all constructs made and used in this study.

Recombinant proteins, antibodies, and egg extract generation

All TPX2 constructs were overexpressed in *Escherichia coli* Rosetta 2 cells (EMD Millipore) for 16–18 h at 16°C in Terrific Broth media and lysed (EmulsiFlex; Avestin). TPX2 proteins were purified with affinity chromatography via a GST tag (GSTrap column; GE Healthcare) or via a His tag (HisTrap column; GE Healthcare). All TPX2 proteins were purified further via cation-exchange chromatography (Mono S or HiTrap SP column; GE Healthcare) and subsequently dialyzed overnight into CSF-XB with 10% sucrose (100 mM KCl, 1 mM $MgCl_2$, 0.1 mM $CaCl_2$, 10 mM Hepes, 4 mM EGTA, and 300 mM sucrose, pH 7.8). Untagged TPX2 α3, α3–α4, α5–α6, α7, α5–α7, and α3–α7, were purified by cleaving the His6-GFP- or His6-mCherry tag with TEV protease after elution from the HisTrap column. The cleaved tags and His6-tagged TEV were removed via a second HisTrap column, and TPX2 proteins were dialyzed into CSF-XB with 10% sucrose. To introduce AzidoPhe, TPX2 constructs were overexpressed in *E. coli* BL21(DE3) cells (New England Biolabs, Inc.), which were cotransformed with the pEVOL-pAzF plasmid (Young et al., 2010). Expression was induced with IPTG, 0.2% arabinose, and 3% p-azidophenylalanine at 16°C for 18 h. Single-site mutant constructs were purified via affinity chromatography (NiNTA agarose; QIAGEN) and dialyzed overnight into CSF-XB with 10% sucrose. EB1-GFP (vector from Albee and Wiese, 2008), EB1-mCherry (mCherry cloned into GFP slot via restriction sites HindIII and BsrGI), and RanQ69L (vector from J. Wilbur and R. Heald [University of California, Berkeley, Berkeley, CA] based on Palacios et al. [1996] and Weis et al. [1996]) were also overexpressed in *E. coli* Rosetta 2 cells (EMD Millipore) for 16–18 h at 16°C in TB media. These proteins were purified with affinity chromatography via a His tag (HisTrap column; GE Healthcare). The purification of RanQ69L was done in the presence of 200 µM GTP, and it included a final incubation with 10-fold molar excess GTP for 60 min. All proteins were dialyzed overnight into CSF-XB with 10% sucrose, flash-frozen in liquid nitrogen, and stored at −80°C. Purified GST-tagged *X. laevis* TPX2 (C-terminal fragment 320–716) protein was used to produce rabbit polyclonal anti–TPX2 antibody serum (Yenzyme). Purified His-tagged *X. laevis* Haus 1, Haus 8, and Haus 6 (C-terminal fragment 624–991) proteins were used to produce rabbit polyclonal anti-H1, anti-H6, and anti-H8 antibody sera (Genscript). Anti–TPX2, anti–H1, anti–H6, and anti–H8 antibodies were purified from serum with an antigen-coupled matrix (Affi-Gel 10 or 15; Bio-Rad). Mouse anti–γ-tubulin (GTU88; Sigma-Aldrich), mouse anti–GCP5 (E-1; Santa Cruz Biotechnology, Inc.), and rabbit anti-GFP (ab290; Abcam) antibodies were purchased. CSF extracts were prepared from *X. laevis* oocytes as described previously (Murray and Kirschner, 1989) and either used immediately or subjected to immunodepletions (Petry et al., 2011).

CD spectroscopy

Untagged TPX2 α3, α3–α4, α5–α6, α7, α3–α7, and α5–α7 were dialyzed overnight into 10 mM KPO_4, pH 7.4, with 100 mM potassium fluorideand passed through 0.22-µm filters (EMD Millipore). CD spectra were recorded on a Chirascan-Plus CD Spectrometer (Applied Photosystems) over the wavelength range of 200 to 260 nm with 0.1-mm path length at 20°C. All spectra were collected with a 1-nm bandwidth and a 5-s sampling time per point. Final experimental spectra are the result of averaging 10 scans and subtracting the blank spectra performed with buffer only. Secondary structure content was estimated from the CD spectra (200–240 nm) using an online tool that relies on the K2D3 method (Louis-Jeune et al., 2012).

Assay setup, microscopy, and image analysis

Branching MT nucleation was assayed as previously described (Petry et al., 2013). In brief, all reactions were performed in the presence of 0.5 mM vanadate (sodium orthovanadate; New England Biolabs, Inc.). All TPX2 constructs, except the single-site mutants, were tested at a final concentration of 0.75 µM, 1 µM, and 2 µM. All TPX2 single-site mutants were tested at a final concentration of 1 µM and 2 µM. For control experiments, equivalent volumes of CSF-XB were used. Depending on the experiment, 10 µM RanQ69L was further added. In most cases, the extract was supplemented with 0.86 µM Alexa Fluor 568–labeled porcine brain tubulin and 85 nM EB1-GFP. When GFP-tagged TPX2 constructs were tested, the extract was supplemented with 0.86 µM Cy5-labeled porcine brain tubulin and 170 nM EB1-mCherry. When mCherry-tagged TPX2 constructs were tested, the extract was supplemented with 0.86 µM Cy5-labeled porcine brain tubulin and 85 nM EB1-GFP. The reaction mixture was prepared on ice and 5 µl pipetted into a flow cell to start the reaction. Imaging was performed with TIRF microscopy on a Ti microscope (Nikon) equipped with an Andor Zyla sCMOS camera and a 100× 1.49 NA TIRF oil objective. All reactions were imaged at room temperature (16–18°C) using NIS-Elements software (Nikon). TPX2 truncation constructs and domain deletion constructs were imaged and analyzed in the following way. Dual-color images were acquired every 2 s. The quantification of MT number per frame was performed in the following order using MATLAB. EB1-GFP intensity of an image sequence was homogenized by dividing a blank background image that was blurred by a Gaussian kernel of 20 pixels. Immotile features were then discarded by applying a temporal median filter spanning five to six frames. EB1 comets, which highlight individual growing MTs, were detected and tracked by the MT plus-end tracking module of uTrack (Applegate et al., 2011). The MT tracks were then counted for each frame to obtain nucleation kinetics. Means were obtained for experiments that had two quantified replicates, and in these cases, absolute error was calculated. These tracks were also

used to obtain mean MT growth speeds throughout the entire image sequence. Three independent fields of view were simultaneously imaged every 8 s for single-site mutants of TPX2 α5–α7. EB1-mCherry intensity of the image sequence was homogenized as described above. EB1 particles were then enhanced by applying the Laplacian of Gaussian filter of two pixels and detected by the MT plus-end detection module of uTrack. Means were obtained for three different fields of view, and standard deviation was calculated. All final images and movies were processed using ImageJ software (Schneider et al., 2012). All extract experiments and quantification of MT number were performed at least three times with different extracts.

Immunoprecipitation

1 µM GFP-TPX2 constructs or GFP protein was added to 150 µl extract and incubated at room temperature for 10 min. Protein A Dynabeads (Invitrogen) coupled with rabbit anti–GFP antibody (Abcam) were gently mixed with extract and allowed to bind for 1 h at 4°C on a rotating wheel. For the immunoprecipitation of endogenous TPX2, 150 µl extract with 10 µM RanQ69L was incubated at room temperature for 10 min. In this experiment, RanQ69L was added to release TPX2 from importin α/β inhibition. Protein A Dynabeads (Invitrogen) coupled with rabbit anti–TPX2 antibody were gently mixed with this extract for 1 h at 4°C on a rotating wheel. All beads were retrieved using a magnet, washed twice with CSF-XB with 10% sucrose, and boiled with SDS-PAGE sample buffer, and the supernatant was separated on an SDS-PAGE gel followed by Western blotting.

MT co-sedimentation and bundling

Porcine brain tubulin was polymerized in BRB80 (80 mM Pipes, 1 mM $MgCl_2$, and 1 mM EGTA, pH 6.8) with 1 mM GTP and 1 mM DTT for 20 min at 37°C and MTs stabilized with 50 µM Taxol. MTs were centrifuged in a TLA 100 rotor at 270,000 *g* for 15 min at room temperature. The MT pellet was resuspended in BRB80 with 40 µM Taxol. 1 µM precleared TPX2 construct was incubated with MT solution (8 µM tubulin) for 20 min at room temperature or in buffer without MTs. The concentration of TPX2 motif deletion mutants and the single-site mutants was 0.5 µM, and the concentration of tubulin in the MT solution was 4 µM. Samples were centrifuged through a 40% glycerol-BRB80 cushion containing 10 µM Taxol in a TLA100 rotor at 270,000 *g* for 15 min at room temperature. After centrifugation, the supernatant fraction was removed from the top (same volume as the original reaction added to the cushion). The pellets were resuspended in the same volume as the supernatant using cold BRB80 with 10 mM $CaCl_2$. Samples were separated by SDS-PAGE and stained with SYPRO-Ruby or detected via Western blotting. For the TPX2 truncated constructs, fraction bound was calculated by dividing the protein intensity in the pellet lane by the total intensity in both the pellet and the supernatant. Fraction bound was averaged over two independent experiments, and standard deviation was calculated. To assess MT bundling, 1.7 mg/ml unlabeled, together with 0.17 mg/ml Cy5-labeled, porcine brain tubulin was polymerized in BRB80 and 1 mM GMPCPP for 1 h at 37°C. MTs were diluted 100× in BRB80 and incubated with an equal volume of 1 µM of each TPX2 construct at room temperature for 5 min. The reactions were flowed into flow chambers and imaged using TIRF microscopy.

MT nucleation in vitro

MT assembly reactions consisted of 30 µM bovine tubulin (PurSolutions) containing 10% Cy5-labeled porcine brain tubulin and 1 mM GTP in BRB80. To remove any preformed tubulin aggregates, the tubulin assembly mix was centrifuged in a TLA100 rotor at 270,000 *g* for 15 min at 4°C. Samples were supplemented with 800 or 200 nM TPX2 protein in BRB80 or with buffer alone as a control. Reactions were incubated for 15 min at 37°C, fixed with 1% glutaraldehyde, and spun down onto poly-lysine treated coverslips. Samples were imaged using epifluorescence microscopy.

SEC-MALS

35 µM His6-mCherry-tagged TPX2 α3–α7 and35 µM untagged TPX2 α5–α7 were subjected to SEC using a Superdex 200 10/30 GL column (GE Healthcare) equilibrated with CSF-XB at 4°C. The eluate was directed to a DAWN HELEOS-II MALS instrument in tandem with an OptiLab TrEX differential refractometer for real-time analysis. Molar mass was calculated using ASTRA 6.0 (Wyatt Technology) software package. For testing the interaction between TPX2 and tubulin, 10 µM His6-mCherry-tagged TPX2 α3–α7 and 10 µM His-6-GFP-tagged TPX2 α5–α7 were buffer-exchanged into ice-cold BRB80 with 6 mM BME and then centrifuged at 270,00 *g* for 15 min at 4°C. Porcine brain tubulin at 0.7 mg/ml in BRB80 with 1 mM GTP was also centrifuged with the above parameters. Both TPX2 proteins and tubulin were diluted twofold in BRB80 with 6 mM BME and individually run on a Superdex 200 10/30 GL column equilibrated with BRB80. Subsequently, both TPX2 proteins were separately mixed in equal volume with the precleared tubulin, incubated on ice for 20 min, and also analyzed via SEC. Absorbance at 280, 488, and 561 nm was simultaneously measured for all samples eluting from the column.

Online supplemental material

Fig. S1 shows the complete sequence of *X. laevis* TPX2, highlighting the different domains, motifs, and predicted secondary structure. Fig. S2 depicts that TPX2 α5–α7 is the minimal construct that can substitute endogenous TPX2. Fig. S3 shows that in the absence of the augmin complex, TPX2 is unable to activate MT nucleation in extract. Fig. S4 depicts that TPX2 α3–α7 and TPX2 α5–α7 are monomeric in solution as measured by SEC-MALS and that they do not interact with dimeric tubulin. Fig. S5 shows that deletion and single-site mutants of TPX2 α5–α7 are still able to bind MTs in vitro and that a strong interaction between TPX2 and augmin is not detectable using immunoprecipitation from extract. Video 1 displays branching MT nucleation in extract with all truncated TPX2 constructs in Fig. 1. Video 2 shows branching MT nucleation in extract for TPX2 constructs with motif deletions in Fig. 4. Video 3 depicts branching MT nucleation in extract initiated by TPX2 constructs with single-site mutations in Fig. 5. Table S1 lists details for all the TPX2 constructs generated and used in this study.

Acknowledgments

We would like to thank David Octeau, Michael Rale, Ping Xu, and Matthew King for help with cloning, expression, and purification of various TPX2 constructs and with antibody preparation, Dr. Joshua Shaevitz for his advice on image analysis, and Dr. Simone Reber and Dr. Jay Gatlin for critical reading of the manuscript and helpful comments.

This work was supported by the National Institutes of Health/National Institute of General Medical Sciences (4R00GM100013), the Pew Scholars Program in the Biomedical Sciences, the Sidney Kimmel Foundation, and the David and Lucile Packard Foundation (all to S. Petry), a Gilliam Fellowship for Advanced Study by the Howard Hughes Medical Institute (to R. Alfaro-Aco), and a Graduate Research Fellowship by the National Science Foundation (to R. Alfaro-Aco).

The authors declare no competing financial interests.

Author contributions: R. Alfaro-Aco designed and performed research, analyzed data, and wrote the manuscript; A. Thawani designed, per-

formed, and analyzed experiments involving kinetics measurements; and S. Petry contributed to research design and writing the manuscript.

Submitted: 17 July 2016
Revised: 3 November 2016
Accepted: 9 January 2017

References

Albee, A.J., and C. Wiese. 2008. Xenopus TACC3/maskin is not required for microtubule stability but is required for anchoring microtubules at the centrosome. *Mol. Biol. Cell.* 19:3347–3356. http://dx.doi.org/10.1091/mbc.E07-11-1204

Applegate, K.T., S. Besson, A. Matov, M.H. Bagonis, K. Jaqaman, and G. Danuser. 2011. plusTipTracker: Quantitative image analysis software for the measurement of microtubule dynamics. *J. Struct. Biol.* 176:168–184. http://dx.doi.org/10.1016/j.jsb.2011.07.009

Balchand, S.K., B.J. Mann, J. Titus, J.L. Ross, and P. Wadsworth. 2015. TPX2 inhibits Eg5 by interactions with both motor and microtubule. *J. Biol. Chem.* 290:17367–17379. http://dx.doi.org/10.1074/jbc.M114.612903

Brunet, S., T. Sardon, T. Zimmerman, T. Wittmann, R. Pepperkok, E. Karsenti, and I. Vernos. 2004. Characterization of the TPX2 domains involved in microtubule nucleation and spindle assembly in *Xenopus* egg extracts. *Mol. Biol. Cell.* 15:5318–5328. http://dx.doi.org/10.1091/mbc.E04-05-0385

Choi, Y.K., P. Liu, S.K. Sze, C. Dai, and R.Z. Qi. 2010. CDK5RAP2 stimulates microtubule nucleation by the γ-tubulin ring complex. *J. Cell Biol.* 191:1089–1095. http://dx.doi.org/10.1083/jcb.201007030

Crooks, G.E., G. Hon, J.M. Chandonia, and S.E. Brenner. 2004. WebLogo: a sequence logo generator. *Genome Res.* 14:1188–1190. http://dx.doi.org/10.1101/gr.849004

Drozdetskiy, A., C. Cole, J. Procter, and G.J. Barton. 2015. JPred4: A protein secondary structure prediction server. *Nucleic Acids Res.* 43(W1):W389–W394. http://dx.doi.org/10.1093/nar/gkv332

Eckerdt, F., P.A. Eyers, A.L. Lewellyn, C. Prigent, and J.L. Maller. 2008. Spindle pole regulation by a discrete Eg5-interacting domain in TPX2. *Curr. Biol.* 18:519–525. http://dx.doi.org/10.1016/j.cub.2008.02.077

Eyers, P.A., and J.L. Maller. 2004. Regulation of *Xenopus* Aurora A activation by TPX2. *J. Biol. Chem.* 279:9008–9015. http://dx.doi.org/10.1074/jbc.M312424200

Fong, K.W., Y.K. Choi, J.B. Rattner, and R.Z. Qi. 2008. CDK5RAP2 is a pericentriolar protein that functions in centrosomal attachment of the γ-tubulin ring complex. *Mol. Biol. Cell.* 19:115–125. http://dx.doi.org/10.1091/mbc.E07-04-0371

Goshima, G., M. Mayer, N. Zhang, N. Stuurman, and R.D. Vale. 2008. Augmin: A protein complex required for centrosome-independent microtubule generation within the spindle. *J. Cell Biol.* 181:421–429. http://dx.doi.org/10.1083/jcb.200711053

Gruss, O.J., R.E. Carazo-Salas, C.A. Schatz, G. Guarguaglini, J. Kast, M. Wilm, N. Le Bot, I. Vernos, E. Karsenti, and I.W. Mattaj. 2001. Ran induces spindle assembly by reversing the inhibitory effect of importin α on TPX2 activity. *Cell.* 104:83–93. http://dx.doi.org/10.1016/S0092-8674(01)00193-3

Helmke, K.J., and R. Heald. 2014. TPX2 levels modulate meiotic spindle size and architecture in *Xenopus* egg extracts. *J. Cell Biol.* 206:385–393. http://dx.doi.org/10.1083/jcb.201401014

Kollman, J.M., J.K. Polka, A. Zelter, T.N. Davis, and D.A. Agard. 2010. Microtubule nucleating γ-TuSC assembles structures with 13-fold microtubule-like symmetry. *Nature.* 466:879–882. http://dx.doi.org/10.1038/nature09207

Kufer, T.A., H.H. Silljé, R. Körner, O.J. Gruss, P. Meraldi, and E.A. Nigg. 2002. Human TPX2 is required for targeting Aurora-A kinase to the spindle. *J. Cell Biol.* 158:617–623. http://dx.doi.org/10.1083/jcb.200204155

Kwon, T., M.I. Chung, R. Gupta, J.C. Baker, J.B. Wallingford, and E.M. Marcotte. 2014. Identifying direct targets of transcription factor Rfx2 that coordinate ciliogenesis and cell movement. *Genom. Data.* 2:192–194. http://dx.doi.org/10.1016/j.gdata.2014.06.015

Lawo, S., M. Bashkurov, M. Mullin, M.G. Ferreria, R. Kittler, B. Habermann, A. Tagliaferro, I. Poser, J.R. Hutchins, B. Hegemann, et al. 2009. HAUS, the 8-subunit human Augmin complex, regulates centrosome and spindle integrity. *Curr. Biol.* 19:816–826. http://dx.doi.org/10.1016/j.cub.2009.04.033

Lin, T.C., A. Neuner, Y.T. Schlosser, A.N. Scharf, L. Weber, and E. Schiebel. 2014. Cell-cycle dependent phosphorylation of yeast pericentrin regulates γ-TuSC-mediated microtubule nucleation. *eLife.* 3:e02208. http://dx.doi.org/10.7554/eLife.02208

Liu, P., Y.K. Choi, and R.Z. Qi. 2014. NME7 is a functional component of the γ-tubulin ring complex. *Mol. Biol. Cell.* 25:2017–2025. http://dx.doi.org/10.1091/mbc.E13-06-0339

Louis-Jeune, C., M.A. Andrade-Navarro, and C. Perez-Iratxeta. 2012. Prediction of protein secondary structure from circular dichroism using theoretically derived spectra. *Proteins.* 80:374–381. http://dx.doi.org/10.1002/prot.23188

Ma, N., U.S. Tulu, N.P. Ferenz, C. Fagerstrom, A. Wilde, and P. Wadsworth. 2010. Poleward transport of TPX2 in the mammalian mitotic spindle requires dynein, Eg5, and microtubule flux. *Mol. Biol. Cell.* 21:979–988. http://dx.doi.org/10.1091/mbc.E09-07-0601

Moritz, M., Y. Zheng, B.M. Alberts, and K. Oegema. 1998. Recruitment of the γ-tubulin ring complex to *Drosophila* salt-stripped centrosome scaffolds. *J. Cell Biol.* 142:775–786. http://dx.doi.org/10.1083/jcb.142.3.775

Murphy, S.M., A.M. Preble, U.K. Patel, K.L. O'Connell, D.P. Dias, M. Moritz, D. Agard, J.T. Stults, and T. Stearns. 2001. GCP5 and GCP6: Two new members of the human γ-tubulin complex. *Mol. Biol. Cell.* 12:3340–3352. http://dx.doi.org/10.1091/mbc.12.11.3340

Murray, A.W., and M.W. Kirschner. 1989. Cyclin synthesis drives the early embryonic cell cycle. *Nature.* 339:275–280. http://dx.doi.org/10.1038/339275a0

Oegema, K., C. Wiese, O.C. Martin, R.A. Milligan, A. Iwamatsu, T.J. Mitchison, and Y. Zheng. 1999. Characterization of two related *Drosophila* γ-tubulin complexes that differ in their ability to nucleate microtubules. *J. Cell Biol.* 144:721–733. http://dx.doi.org/10.1083/jcb.144.4.721

Palacios, I., K. Weis, C. Klebe, I.W. Mattaj, and C. Dingwall. 1996. RAN/TC4 mutants identify a common requirement for snRNP and protein import into the nucleus. *J. Cell Biol.* 133:485–494. http://dx.doi.org/10.1083/jcb.133.3.485

Petry, S., C. Pugieux, F.J. Nédélec, and R.D. Vale. 2011. Augmin promotes meiotic spindle formation and bipolarity in *Xenopus* egg extracts. *Proc. Natl. Acad. Sci. USA.* 108:14473–14478. http://dx.doi.org/10.1073/pnas.1110412108

Petry, S., A.C. Groen, K. Ishihara, T.J. Mitchison, and R.D. Vale. 2013. Branching microtubule nucleation in *Xenopus* egg extracts mediated by augmin and TPX2. *Cell.* 152:768–777. http://dx.doi.org/10.1016/j.cell.2012.12.044

Reid, T.A., B.M. Schuster, B.J. Mann, S.K. Balchand, M. Plooster, M. McClellan, C.E. Coombes, P. Wadsworth, and M.K. Gardner. 2016. Suppression of microtubule assembly kinetics by the mitotic protein TPX2. *J. Cell Sci.* 129:1319–1328. http://dx.doi.org/10.1242/jcs.178806

Roostalu, J., N.I. Cade, and T. Surrey. 2015. Complementary activities of TPX2 and chTOG constitute an efficient importin-regulated microtubule nucleation module. *Nat. Cell Biol.* 17:1422–1434. http://dx.doi.org/10.1038/ncb3241

Samejima, I., V.J. Miller, L.M. Groocock, and K.E. Sawin. 2008. Two distinct regions of Mto1 are required for normal microtubule nucleation and efficient association with the γ-tubulin complex in vivo. *J. Cell Sci.* 121:3971–3980. http://dx.doi.org/10.1242/jcs.038414

Sanchez-Pulido, L., L. Perez, S. Kuhn, I. Vernos, and M.A. Andrade-Navarro. 2016. The C-terminal domain of TPX2 is made of α-helical tandem repeats. *BMC Struct. Biol.* 16:17. http://dx.doi.org/10.1186/s12900-016-0070-8

Schatz, C.A., R. Santarella, A. Hoenger, E. Karsenti, I.W. Mattaj, O.J. Gruss, and R.E. Carazo-Salas. 2003. Importin α-regulated nucleation of microtubules by TPX2. *EMBO J.* 22:2060–2070. http://dx.doi.org/10.1093/emboj/cdg195

Schneider, C.A., W.S. Rasband, and K.W. Eliceiri. 2012. NIH Image to ImageJ: 25 years of image analysis. *Nat. Methods.* 9:671–675. http://dx.doi.org/10.1038/nmeth.2089

Scrofani, J., T. Sardon, S. Meunier, and I. Vernos. 2015. Microtubule nucleation in mitosis by a RanGTP-dependent protein complex. *Curr. Biol.* 25:131–140. http://dx.doi.org/10.1016/j.cub.2014.11.025

Sievers, F., A. Wilm, D. Dineen, T.J. Gibson, K. Karplus, W. Li, R. Lopez, H. McWilliam, M. Remmert, J. Söding, et al. 2011. Fast, scalable generation of high-quality protein multiple sequence alignments using Clustal Omega. *Mol. Syst. Biol.* 7:539. http://dx.doi.org/10.1038/msb.2011.75

Tan, S., R.C. Kern, and W. Selleck. 2005. The pST44 polycistronic expression system for producing protein complexes in *Escherichia coli*. *Protein Expr. Purif.* 40:385–395. http://dx.doi.org/10.1016/j.pep.2004.12.002

Trieselmann, N., S. Armstrong, J. Rauw, and A. Wilde. 2003. Ran modulates spindle assembly by regulating a subset of TPX2 and Kid activities including Aurora A activation. *J. Cell Sci.* 116:4791–4798. http://dx.doi.org/10.1242/jcs.00798

Tsai, M.Y., C. Wiese, K. Cao, O. Martin, P. Donovan, J. Ruderman, C. Prigent, and Y. Zheng. 2003. A Ran signalling pathway mediated by the mitotic kinase Aurora A in spindle assembly. *Nat. Cell Biol.* 5:242–248. http://dx.doi.org/10.1038/ncb936

Uehara, R., R.S. Nozawa, A. Tomioka, S. Petry, R.D. Vale, C. Obuse, and G. Goshima. 2009. The augmin complex plays a critical role in spindle microtubule generation for mitotic progression and cytokinesis in human cells. *Proc. Natl. Acad. Sci. USA.* 106:6998–7003. http://dx.doi.org/10.1073/pnas.0901587106

Vale, R.D., and R.A. Milligan. 2000. The way things move: Looking under the hood of molecular motor proteins. *Science.* 288:88–95. http://dx.doi.org/10.1126/science.288.5463.88

Weis, K., C. Dingwall, and A.I. Lamond. 1996. Characterization of the nuclear protein import mechanism using Ran mutants with altered nucleotide binding specificities. *EMBO J.* 15:7120–7128.

Widlund, P.O., J.H. Stear, A. Pozniakovsky, M. Zanic, S. Reber, G.J. Brouhard, A.A. Hyman, and J. Howard. 2011. XMAP215 polymerase activity is built by combining multiple tubulin-binding TOG domains and a basic lattice-binding region. *Proc. Natl. Acad. Sci. USA.* 108:2741–2746. http://dx.doi.org/10.1073/pnas.1016498108

Wieczorek, M., S. Bechstedt, S. Chaaban, and G.J. Brouhard. 2015. Microtubule-associated proteins control the kinetics of microtubule nucleation. *Nat. Cell Biol.* 17:907–916. http://dx.doi.org/10.1038/ncb3188

Wittmann, T., M. Wilm, E. Karsenti, and I. Vernos. 2000. TPX2, A novel *Xenopus* MAP involved in spindle pole organization. *J. Cell Biol.* 149:1405–1418. http://dx.doi.org/10.1083/jcb.149.7.1405

Young, T.S., I. Ahmad, J.A. Yin, and P.G. Schultz. 2010. An enhanced system for unnatural amino acid mutagenesis in *E. coli*. *J. Mol. Biol.* 395:361–374. http://dx.doi.org/10.1016/j.jmb.2009.10.030

Zheng, Y., M.L. Wong, B. Alberts, and T. Mitchison. 1995. Nucleation of microtubule assembly by a γ-tubulin-containing ring complex. *Nature.* 378:578–583. http://dx.doi.org/10.1038/378578a0